Biosensors and Bioelectronics 100 (2018) 85–88

Contents lists available at ScienceDirect

Biosensors and Bioelectronics

journal homepage: www.elsevier.com/locate/bios

Novel graphene-based biosensor for early detection of Zika virus infection

Savannah Afsahi[a], Mitchell B. Lerner[a], Jason M. Goldstein[b], Joo Lee[b], Xiaoling Tang[b], Dennis A. Bagarozzi Jr.[b], Deng Pan[a], Lauren Locascio[a], Amy Walker[a], Francie Barron[a], Brett R. Goldsmith[a,*]

[a] Nanomedical Diagnostics Inc., 6185 Cornerstone Court East Suite #110, San Diego, CA 92121, USA
[b] Reagent and Diagnostic Services Branch, Division of Scientific Resources, National Center for Emerging and Zoonotic Infectious Diseases (NCEZID), Centers for Disease Control and Prevention, 1600 Clifton Road NE, Atlanta, GA 30333, USA

ARTICLE INFO

Keywords:
Graphene
Biosensor
Zika
Field effect biosensing
FEB

ABSTRACT

We have developed a cost-effective and portable graphene-enabled biosensor to detect Zika virus with a highly specific immobilized monoclonal antibody. Field Effect Biosensing (FEB) with monoclonal antibodies covalently linked to graphene enables real-time, quantitative detection of native Zika viral (ZIKV) antigens. The percent change in capacitance in response to doses of antigen (ZIKV NS1) coincides with levels of clinical significance with detection of antigen in buffer at concentrations as low as 450 pM. Potential diagnostic applications were demonstrated by measuring Zika antigen in a simulated human serum. Selectivity was validated using Japanese Encephalitis NS1, a homologous and potentially cross-reactive viral antigen. Further, the graphene platform can simultaneously provide the advanced quantitative data of nonclinical biophysical kinetics tools, making it adaptable to both clinical research and possible diagnostic applications. The speed, sensitivity, and selectivity of this first-of-its-kind graphene-enabled Zika biosensor make it an ideal candidate for development as a medical diagnostic test.

1. Introduction

Zika is a vector borne viral infection originating in the Zika Forest of Uganda in the mid-20th century (Sikka et al., 2016). Since its discovery, there have been several significant outbreaks of Zika, most recently in 2015 in North and South America including the United States (Peterson et al., 2016). The long-term effects of Zika include severe brain defects in fetuses (Rasmussen et al., 2016) and Guillain-Barre Syndrome in adults (Ladhani et al., 2016). As a result, the Zika virus epidemic has been a growing concern for public health in the United States. Over 41,000 cases of Zika virus infection have been reported since January 2015 within the United States and its territories, of which 3461 cases are pregnant women (Centers for Disease Control, 2017). The current diagnostic standards for Zika detection are RNA Nucleic Acid Testing (RNA NAT), Trioplex rRT-PCR, or the Zika IgM Antibody Capture Enzyme-Linked Immunosorbent Assay (Zika MAC-ELISA) in urine, serum, or cerebrospinal fluid (Huzly et al., 2016; Lanciotti et al., 2008). However, due to cross-reactivity with co-circulating viruses, such as dengue and Japanese encephalitis (JEV) (Sironi et al., 2016; Xu et al., 2016), the confirmation rate of presumptive positive results is less than 50% for the commercial IgM capture ELISA (Food and Drug Administration, 2016). Both timely and accurate diagnostic capabilities from emerging technologies are needed to combat this public health threat.

Highly sensitive nanomaterials show promise as biosensors by affording lower limits of detection with better selectivity than traditional assays. A promising biosensor candidate, graphene, is a single layer, two-dimensional sheet of hexagonally arranged carbon atoms first experimentally isolated in 2004 (Geim and Novoselov, 2007; Novoselov et al., 2004). As a conductive, two-dimensional material, every atom in a graphene sheet is in direct contact with its environment and responds to electrostatic fluctuations, making it an ideal candidate for sensing applications (Zhu et al., 2013). Indeed, graphene has been incorporated into sensors of all varieties, including pressure sensors (Zhu et al., 2013), chemical vapor sensors (Esfandiar et al., 2013; Lu et al., 2010), optical sensors, (Lu et al., 2012) and biomolecular sensors (Lerner et al., 2014).

We have recently demonstrated use of a commercially available graphene chip as a biosensor, with read out by portable electronic hardware (Lerner et al., 2016). Graphene is selected as the base material for our platform over other nanomaterials because of this extensive publication history of sensor devices coupled with recent

* Corresponding author.
E-mail address: brgoldsmith@nanomedicaldiagnostics.com (B.R. Goldsmith).

http://dx.doi.org/10.1016/j.bios.2017.08.051
Received 22 June 2017; Received in revised form 17 August 2017; Accepted 23 August 2017
Available online 24 August 2017

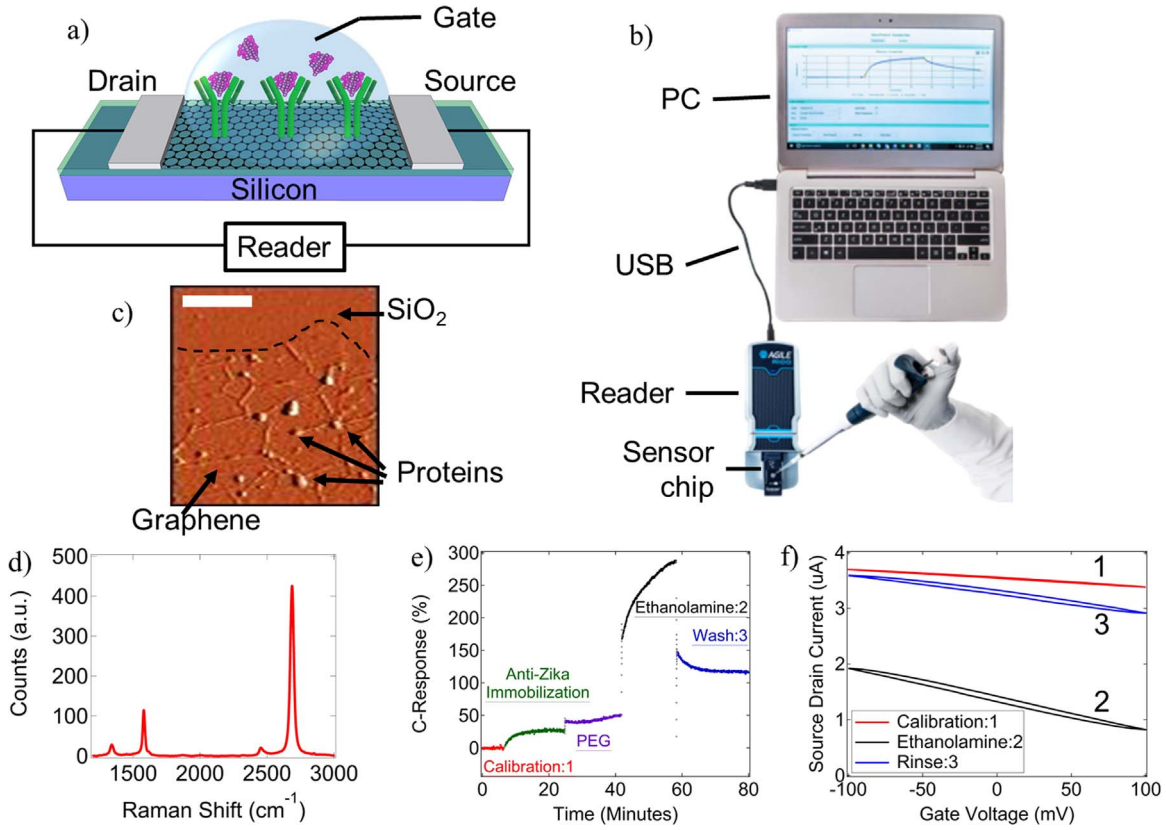

Fig. 1. (a) Diagram of the sensor element of the graphene biosensor chip. Antibodies are immobilized on pristine graphene using a zero-length linker. Along with the PEG block, these antibodies form the dielectric in a liquid gated transistor with a graphene channel. (b) Illustration of the entire sensor chip system, incorporating the sensor chip, reader electronics and digital control, and PC running control and data presentation software. (c) AFM image of the graphene after successful protein attachment, scale bar is 1 μm and Z height is 10 nm. (d) Raman spectrum after device fabrication demonstrating low D/G ratio, which indicates high quality graphene. (e) Percent change in capacitance during target immobilization and quenching on the graphene biosensor chip surface. (f) I-Vg curves at different immobilization steps. The dramatic steepening of the I-Vg slope indicates substantial change in the surface chemistry and increased sensitivity of the biosensor.

availability of graphene biosensor chips that have been processed through commercial fab, packaging and QA processes (Lerner et al., 2016). Use of commercially available biosensor chips rather than lab built biosensor chips allows us to evaluate the material and device characteristics using scaled production, closer to what is needed for a potential fielded diagnostic device compared to a laboratory constructed device. These chips are modified here to demonstrate sensitive and specific detection of Zika viral nonstructural protein 1 (ZIKV NS1).

2. Materials and methods

2.1. Graphene biosensor fabrication

Biosensor chips are fabricated at a commercial foundry as described previously (Lerner et al., 2016). Briefly, photolithography and plasma-enhanced CVD is used to pattern and passivate graphene with Ti/Pt leads on 6" silicon wafers (Lerner et al., 2016). High quality, single layer graphene films are grown via CVD on copper foil (Alfa Aesar) and transferred via bubbing transfer (Gao et al., 2012; Kybert et al., 2014). Individual dies are packaged using a chip-on-board process and encapsulated with epoxy to form an exposed well above the graphene biosensor surface.

2.2. Graphene biosensor measurement

Graphene biosensor chips are read using the commercial Agile R100 system (Nanomedical Diagnostics), previously described in detail (Lerner et al., 2016). With this system, graphene biosensor chips are inserted into an electronic reader that applies a source-drain voltage across the graphene channel and a gate voltage between the applied liquid and the drain electrode of the graphene. There are 2 read-out channels available: the I-Response (current through the channel) and the C-Response (capacitance of biosensor to the liquid). In this study, the C-Response channel is used. Control of the system, as well as data readout is performed via the Agile Plus software, which is run on a PC attached to the system via USB, as shown in Fig. 1b.

2.3. Protein Immobilization

Our previously described NHS surface chemistry was used to build sensor chips ready for protein attachment (Afsahi et al., 2017).

The biosensor chips were then functionalized with the target, anti-Zika NS1 mouse mAb 6B1 developed by the Centers for Disease Control (CDC). Anti-Zika NS1 was diluted to a working concentration of 14.6 nM in 1X phosphate buffered saline (PBS) pH 7.4. During immobilization and measurement, 75 μL of all solutions were used on the biosensor chips and incubation steps took place at room temperature. The software was calibrated to baseline in 1X PBS pH 7.4 for 60 s. Anti-Zika NS1 was immobilized on the surface by incubating for 15 min. Polyethylene glycol (PEG) has previously been shown to be an effective block against non-specific interactions in general and specifically when covalently attached to graphene devices (Gao et al., 2016; Liu et al., 2013). Thus, residual active NHS groups were first quenched using 3 mM amino-PEG_5-alcohol (amino-PEG) pH 7.4 (BroadPharm) before a final quench with 1 M Ethanolamine pH 8.5. Each quench step was done for 15 min each, followed by several washes in 1X PBS pH 7.4. The high concentration of PEG used during blocking leads to both covalently linked PEG to the graphene surface and

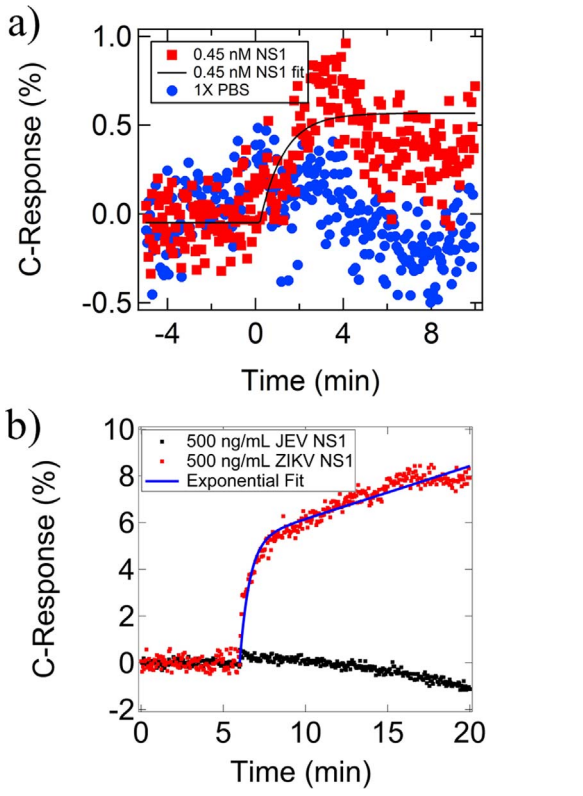

Fig. 2. (a) C-response sensorgram of a graphene biosensor to 0.45 nM ZIKV NS1 in 1X PBS pH 7.4. Control (blue) is a re-application of 1X PBS pH 7.4. (b) Sensorgram of the C-Response during sensing by anti-ZIKV NS1 of 500 ng/mL JEV NS1 versus an equal concentration of ZIKV NS1. Blue line indicates single exponential fit to the ZIKV NS1 response curve. (For interpretation of the references to color in this figure legend, the reader is referred to the web version of this article.)

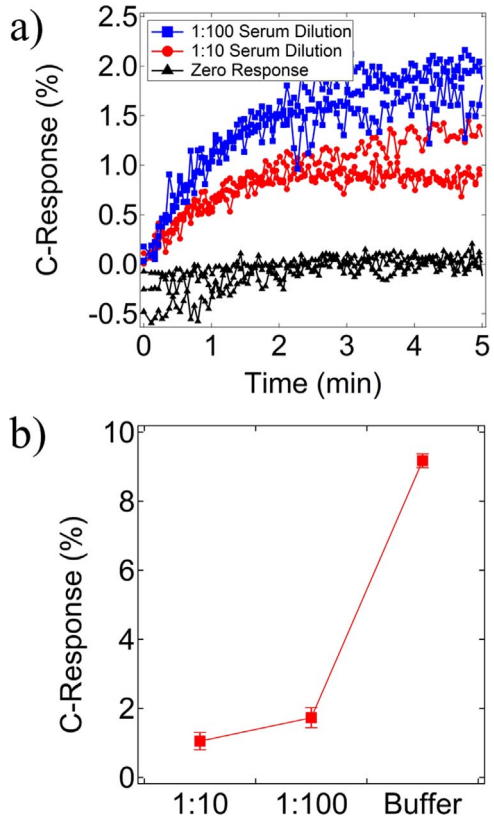

Fig. 3. (a) C-Response from 4 sensor chips each for 1:10 serum dilution with no antigen spike in (zero response), 1:10 serum dilution with 500 ng/mL ZIKV NS1 spike-in, and 1:100 serum dilution with 500 ng/mL ZIKV NS1 spike-in. (b) Change in C-Response with dilution factor. Error bars are standard deviations.

absorbed PEG to the rest of the chip surfaces. This provides both an anti-absorptive to the SiO_2 as well as a stable block on the graphene against non-specific interactions at the surface.

Measurements were performed in an assay buffer of 1X PBS pH 7.4 or a dilution of simulated serum (Cellastim, InVitria) for spike in measurements at 1:10 and 1:100 of serum to 1X PBS pH 7.4. Immediately after immobilization, the biosensor chips were calibrated in assay buffer for 5 min. The ZIKV NS1 recombinant antigen (The Native Antigen Company) was diluted in assay buffer to the desired concentration. Each concentration was applied to individual biosensor chips for at least 5 min to generate a sensor response. A negative control was also conducted using 500 ng/mL Japanese encephalitis (JEV) NS1 recombinant viral antigen (The Native Antigen Company) applied to biosensor chips using the same protocol as the ZIKV NS1 targets.

3. Results and discussion

Graphene quality is indicated by the low D/G ratio (< 0.1) in the Raman spectrum depicted in Fig. 1d. Atomic Force Microscopy (AFM) indicates that target immobilization on the 1.0 nm thick graphene surface (Supplemental Fig. S1) occurs at the optimal density of 5 proteins/μm^2 and thus confirms the change in C-Response after protein immobilization (Fig. 1c).

The graphene biosensor chip relies on Field Effect Biosensing (FEB) technology, whereby the channel current and gate capacitance of a field effect graphene transistor shift reproducibly when appropriate biological targets are immobilized to the surface as the gate dielectric (Fig. 1a). Pristine graphene is functionalized to bind the desired target. The graphene surface is then blocked and passivated to reduce non-specific interactions. Biosensors are monitored throughout this process, as shown in Fig. 1e. Notably, antibody immobilization produced a 20% increase in the capacitance response (Fig. 1e). Further, a 100% increase was seen in the C-Response between the wash step and the calibrated baseline (Fig. 1e). This indicates that irreversible chemical modifications took place on the surface, successfully functionalizing the biosensor. Anti-Zika NS1 has a greater impact on the capacitance of graphene transistors than the source-drain resistance, which is why the C-Response channel was used in this study.

Each of the datapoints in Fig. 1e corresponds to a complete cycle of liquid gate voltage from −100 to 100 mV and back. Fig. 1f shows representative complete current versus gate voltage curves during calibration, quenching, and rinsing. The increase in the I-Vg slope (higher transconductance) implies increased sensitivity of the graphene biosensor.

In developing a clinical diagnostic test, maximizing sensitivity and specificity is critical. The current incidence of Zika infection is unclear due to high rates of cross-reactivity with other co-circulating flavivirus pathogens. To address this, diagnostics target a specific viral protein with unique epitopes. The crystal structure of ZIKV NS1 reveals that the protein C-terminal has electrostatic characteristics that differentiate it from related co-circulating viruses (Song et al., 2016). This unique charge signature allows for development of specific mAbs with limited cross-reactivity among related viruses such as JEV.

Sensitivity of ZIKV NS1 detection on a graphene biosensor chip was determined by running several analyte concentrations. Fig. 2a shows the calibration, response, and exponential sensorgram fit for 0.45 nM ZIKV NS1. The RMS noise level of the Agile R100 system is ± 0.2%. Our previous work measuring Zika antigen in buffer has shown a limit of detection of 0.45 nM ZIKV NS1 in buffer, a significant improvement over other label free techniques such as BLI when using this antibody-antigen system (Afsahi et al., 2017).

To demonstrate the selectivity of anti-Zika NS1 immobilized on graphene based biosensor chips, 500 ng/mL ZIKV NS1 or JEV NS1 was applied to individual biosensor chips functionalized with anti-ZIKV NS1. JEV NS1 shares 56.5% amino acid sequence identity with ZIKV and represents a potential cross-reactive species (Xu et al., 2016). When a single exponential fit was applied to the resulting sensorgram (Fig. 2b), the ZIKV NS1 C-response was 8%. Comparatively, JEV NS1 did not elicit a measurable sensor response when exposed to anti-ZIKV NS1, demonstrating high selectivity for ZIKV NS1 antigen.

Spike-in measurements in simulated serum were performed at 2 dilutions in quadruplicate to demonstrate the potential for optimization of this assay for diagnostic purposes. Sensorgrams are shown in Fig. 3a, and the average responses after 5 min with standard deviations are shown in Fig. 3b. Dilution of serum improved the coefficient of variation percentage (CV%) despite lowering the overall sensor response. Generally, for in vitro diagnostics, CV% should be ≤ 20%, with ≤ 10% being considered a reliable test. However these parameters are based on assay precision in relation to clinical allowable error (Clinical Laboratory Standards Institute, 2012). At 1:10 dilution, the CV is 19.89%, while at 1:100 dilution, the CV is 9.17% (see Supplemental Table S1), which suggests the possibility of a diagnostic valuable in a clinical setting.

4. Conclusions

Emerging epidemics such as Zika drive advances in the medical and research sectors. Interpretation of the results of Zika virus antibody (IgM) tests may be complicated due to high cross-reactivity among related, co-circulating viruses such as JEV. Covalent linkage of anti-Zika NS1 to a graphene biosensor chip enables low cost and portable acquisition of real-time kinetic binding data via FEB technology. The Agile R100 biosensor chip functionalized with anti-Zika NS1 detects ZIKV NS1 at concentrations as low as 0.45 nM. Furthermore, when the device was tested with JEV NS1 there was no measurable cross-reactivity. The LLOD and specificity of the ZIKV NS1 antigen provide an opportunity for early stage detection of active disease in presumptive Zika infection. The Agile R100 FEB platform provides a promising base for development into Zika clinical applications and improved diagnostic testing early in infection.

Acknowledgements

The Centers for Disease Control and Prevention does not endorse any product or service that is directly or indirectly related to this Collaborative Research Agreement. The findings and conclusions in this Report are those of the author(s) and do not necessarily represent the views of the Centers for Disease Control and Prevention.

Funding was provided internally by the collaborating organizations.

Appendix A. Supplementary material

Supplementary data associated with this article can be found in the online version at doi:10.1016/j.bios.2017.08.051.

References

Afsahi, S.J., Locascio, L.E., Pan, D., Gao, Y., Walker, A.E., Barron, F.E., Goldsmith, B.R., Lerner, M.B., 2017. MRS Adv., 1–7.
Centers for Disease Control, 2017. Zika Virus: Case Counts in the US [WWW Document]. May 16, 2017.
Clinical Laboratory Standards Institute, 2012. NCCLS Doc. EP15-A2 25.
Esfandiar, A., Kybert, N.J., Dattoli, E.N., Hee Han, G., Lerner, M.B., Akhavan, O., Irajizad, A., Charlie Johnson, A.T., 2013. Appl. Phys. Lett. 103.
Food and Drug Administration, 2016. FDA Warns Health Care Providers Against Relying Solely on Zika Virus Serological IgM Assay Results. Reminds them to Wait for Confirmatory Test Results Before Making Patient Management Decisions: FDA Safety Communication [WWW Document]. May 16, 2017.
Gao, L., Ren, W., Xu, H., Jin, L., Wang, Z., Ma, T., Ma, L.-P., Zhang, Z., Fu, Q., Peng, L.-M., Bao, X., Cheng, H.-M., 2012. Nat. Commun. 3, 699.
Gao, N., Gao, T., Yang, X., Dai, X., Zhou, W., Zhang, A., Lieber, C.M., 2016. Proc. Natl. Acad. Sci. USA 113, 14633–14638.
Geim, A.K., Novoselov, K.S., 2007. Nat. Mater. 6, 183–191.
Huzly, D., Hanselmann, I., Schmidt-Chanasit, J., Panning, M., 2016. Eurosurveillance 21.
Kybert, N.J., Han, G.H., Lerner, M.B., Dattoli, E.N., Esfandiar, A., Charlie Johnson, A.T., 2014. Nano Res. 7, 95–103.
Ladhani, S.N., O'Connor, C., Kirkbride, H., Brooks, T., Morgan, D., 2016. Arch. Dis. Child. 0, (archdischild–2016–310590).
Lanciotti, R.S., Kosoy, O.L., Laven, J.J., Velez, J.O., Lambert, A.J., Johnson, A.J., Stanfield, S.M., Duffy, M.R., 2008. Emerg. Infect. Dis. 14, 1232–1239.
Lerner, M.B., Matsunaga, F., Han, G.H., Hong, S.J., Xi, J., Crook, A., Perez-Aguilar, J.M., Park, Y.W., Saven, J.G., Liu, R., Johnson, A.T.C., 2014. Nano Lett. 14, 2709–2714.
Lerner, M.B., Pan, D., Gao, Y., Locascio, L.E., Lee, K., Nokes, J., Afsahi, S., Lerner, J.D., Walker, A., Collins, P.G., Oegema, K., Barron, F., Goldsmith, B.R., 2016. Sens. Actuators B Chem., 1–7.
Liu, B., Huang, P.-J.J., Zhang, X., Wang, F., Pautler, R., Ip, A.C., Liu, J., 2013. Anal. Chem. 85, 10045–10050.
Lu, Y., Goldsmith, B.R., Kybert, N.J., Johnson, A.T.C., 2010. Appl. Phys. Lett. 97.
Lu, Y., Lerner, M.B., John Qi, Z., Mitala, J.J., Hsien Lim, J., Discher, B.M., Charlie Johnson, A.T., 2012. Appl. Phys. Lett. 100.
Novoselov, K.S., Geim, A.K., Morozov, S.V., Jiang, D., Zhang, Y., Dubonos, S.V., Grigorieva, I.V., Firsov, A.A., 2004. Science 306, 666–669, (80-.).
Peterson, L., Jamieson, D., Powers, A., Honein, M., 2016. N. Engl. J. Med., 1602113.
Rasmussen, S.A., Jamieson, D.J., Honein, M.A., Petersen, L.R., 2016. N. Engl. J. Med., 1–7.
Sikka, V., Chattu, V., Popli, R., Galwankar, S., Kelkar, D., Sawicki, S., Stawicki, S., Papadimos, T., 2016. J. Glob. Infect. Dis. 8, 3.
Sironi, M., Forni, D., Clerici, M., Cagliani, R., 2016. PLoS Negl. Trop. Dis. 10, 1–18.
Song, H., Qi, J., Haywood, J., Shi, Y., Gao, G.F., 2016. vol. 23, pp. 3–6.
Xu, X., Vaughan, K., Weiskopf, D., Grifoni, A., Diamond, M.S., Sette, A., Peters, B., 2016. PLoS Curr..
Zhu, S.E., Krishna Ghatkesar, M., Zhang, C., Janssen, G.C.A.M., 2013. Appl. Phys. Lett. 102.